science.sciencemag.org/cgi/content/full/science.abb7431/DC1

Supplementary Materials for

Unexpected air pollution with marked emission reductions during the COVID-19 outbreak in China

Tianhao Le*, Yuan Wang*†, Lang Liu*, Jiani Yang, Yuk L. Yung, Guohui Li, John H. Seinfeld

*These authors contributed equally to this work.
†Corresponding author. Email: yuan.wang@caltech.edu

Published 17 June 2020 on *Science* First Release
DOI: 10.1126/science.abb7431

This PDF file includes:

Materials and Methods
Figs. S1 to S9
Tables S1 to S3
References

Materials and Methods

Satellite product

The TROPOMI instrument onboard the Copernicus Sentinel-5P satellite provides daily global coverage of tropospheric column density of NO2 with a spatial resolution 3.5 × 7 km^2 (3.5 × 5.5 km^2 starting from August 6, 2019) with overpass time around 13:30. The TROPOMI NO2 processing system is based on the algorithm developments for the DOMINO-2 product and for the EU QA4ECV NO2 reprocessed dataset for OMI, and has been adapted for TROPOMI. In this study, the tropospheric NO2 column densities were taken from S-5P/TROPOMI Level 2 offline products. The measurements with a Quality Assurance (QA) value less than 0.5 were omitted, which removed the measurements with processing errors, anomalously high signals, and sun glints. We re-gridded the Level 2 product on a 0.03°×0.03° spatial grid which corresponds to 3.3 km in latitude.

The MODIS Level 3 AOD datasets are from Aqua (MYD08_D3) and Terra (MOD08_D3) with 1°×1° spatial resolution. We generate the Level 3 daily map by using the average value of Aqua and Terra measurements. Data can be downloaded from ftp://ladsweb.nascom.nasa.gov/allData/51/MYD08_D3 and ftp://ladsweb.nascom.nasa.gov/allData/51/MOD08_D3, respectively.

Ground station observations

Hourly air quality data have been obtained from the national urban air quality real-time platform released by the China National Environmental Monitoring Station (website: http://106.37.208.233:20035). Information from the national air quality monitoring stations used in this study over four major cities is shown in Table S1. The method of measuring air quality follows the national standard of GB 3095-2012. Measurement of PM2.5 was carried out by the β Ray absorption method and micro-oscillation balance method; measurement of NO2 is by the Chemiluminescence method; measurement of SO2 and O3 is by the UV fluorescence method; measurement of CO is by the non-dispersive infrared absorption method and gas filter correlation infrared absorption method. Monitoring stations usually avoid tall buildings, trees and other potential obstacles that would impede air circulation. The surroundings of air monitoring site have been guaranteed with stable electricity supplies and device maintenance service. Sampling ports are 3 to 15 meters above the ground. The distance between each sampling port exceeds 1 m. Temperature inside the monitoring stations is maintained between 15 and 35 ℃, relative humidity ≤85%, and atmospheric pressure between 80 and 106 kPa.

Reanalysis data

The boundary layer height, precipitation, relative humidity at 1000 hPa and the wind vector w = (u,v) at 10 meters above the ground were taken from the ERA5 reanalysis data with 0.25°×0.25° spatial resolution. ERA5 combines historical observations into global estimates using advanced modelling and data assimilation systems.

WRF-Chem model simulations

The model used in this study is based on a specific version of the WRF-Chem model (*23*) with modification by (*24–27*). The specific WRF-Chem model includes a flexible gas phase chemical module with consideration of different chemical mechanisms and the CMAQ aerosol module (AERO5) developed by US EPA (*28*). The organic aerosols (OA) are simulated using the volatility basis-set (VBS) modeling method, with the secondary OA (SOA) contributions from glyoxal and methylglyoxal. ISORROPIA (Version 1.7) is used to predict the inorganic aerosols, calculating the composition and phase state of an ammonium-sulfate-nitrate-water inorganic aerosol in thermodynamic equilibrium with gas phase precursors (*29*). Three major types of heterogeneous aerosol chemistry are considered: the heterogeneous hydrolysis of N_2O_5 on the surface of deliquescent aerosols to form nitrate, the heterogeneous reaction of SO_2 involving aerosol water to form sulfate, and the heterogeneous reaction of glyoxal and methylglyoxal to form SOA.

The anthropogenic emission inventory is developed by (*30*) with the base year of 2020, including industry, transportation, power plant, residential and agriculture sources. The Model of Emissions of Gases and Aerosols from Nature (MEGAN) is used to calculate the biogenic emissions online (*31*). Biomass burning emissions are potentially important for Asian haze (*32–35*). Fire counts from satellites can partly reflect BB in agricultural activities and wildfires. In the fig. S9, we analyzed the MODIS fire counts during the 2020 city-lockdown period and found very few fire activities in the Beijing-Tianjin-Hebei area. Moreover, the fires were more frequent in the same period of 2019 than that in 2020 over the whole nation. Therefore, we conclude that BB from agriculture and wildfires did not contribute significantly to the haze formation during the 2020-CLD, and we did not consider them in our WRF-Chem simulations. A haze episode from 21 January to 16 February 2020 in the North China Plain is simulated using the WRF-Chem model, and detailed model configuration can be found in Table S2. A series of model sensitivity experiments are conducted, and the experiment descriptions are provided in Table S3.

The mean bias (MB), root mean square error (RMSE) and the index of agreement (IOA) are used to evaluate the model performance in simulating air pollutants.

$$\mathrm{MB} = \frac{1}{\mathrm{N}}\sum_{\mathrm{i}=1}^{\mathrm{N}}(\mathrm{P_i} - \mathrm{O_i})$$

$$\mathrm{RMSE} = \left[\frac{1}{\mathrm{N}}\sum_{\mathrm{i}=1}^{\mathrm{N}}(\mathrm{P_i} - \mathrm{O_i})^2\right]^{\frac{1}{2}}$$

$$\mathrm{IOA} = 1 - \frac{\sum_{\mathrm{i}=1}^{\mathrm{N}}(\mathrm{P_i}-\mathrm{O_i})^2}{\sum_{\mathrm{i}=1}^{\mathrm{N}}(|\mathrm{P_i}-\bar{\mathrm{O}}|+|\mathrm{O_i}-\bar{\mathrm{O}}|)^2}$$

Where P_i and O_i are the simulated and observed variables, respectively. *N* is the total number of the simulations for comparisons, and $\bar{O}$ donates the average of the observations.

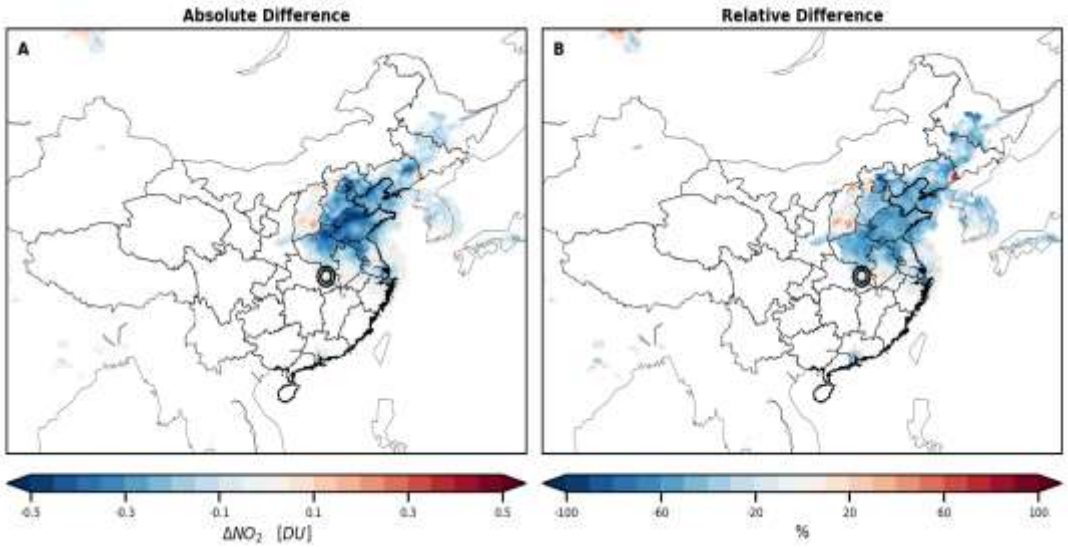

Fig. S1. Comparison of column integrated NO_2 between three weeks during the 2020 lockdown and 2015-2019 climatology using NASA Aura OMI products. Only regions with background NO_2 larger than 0.2 DU are analyzed.

Fig. S2. Spatial distribution of the 1515 state monitoring stations.

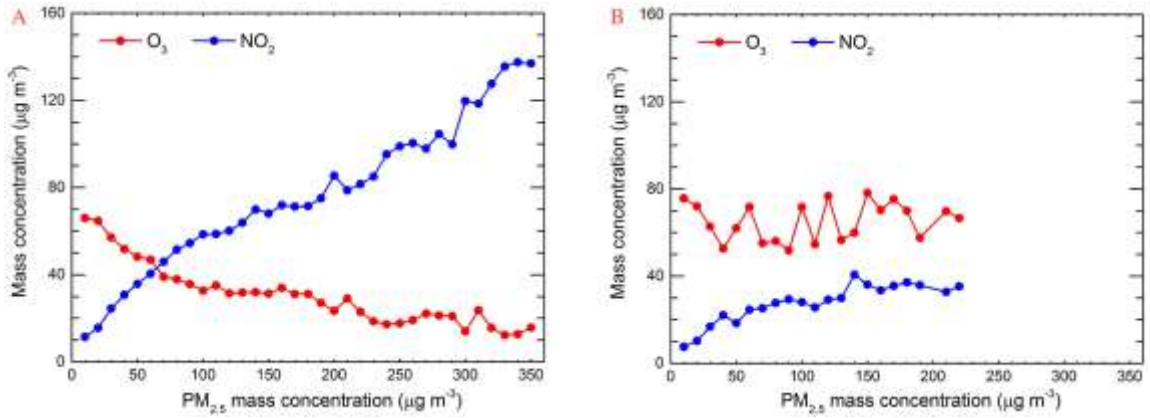

Fig. S3. Daytime variation of ozone and NO_2 (10:00 to 16:00 LST) as a function of $PM_{2.5}$ in the winter from 2015 to 2019 (A) and during 2020-CLD (B). During wintertime in north China, the weak insolation slows the atmospheric photochemistry processes. Therefore, very high NOx emissions in the region cause remarkable ozone titration even during daytime, as shown in A, particularly with increasing $PM_{2.5}$ which further attenuates the incoming solar radiation. However, during 2020-CLD, significant decrease in NOx emissions alleviates the ozone titration, and during haze episodes, the ozone level is much higher than that during the winter from 2015 to 2019. The ozone concentration fluctuates at around 65 μg m^{-3} with $PM_{2.5}$ exceeding 35 μg m^{-3}, caused by complicated nonlinear ozone chemistry.

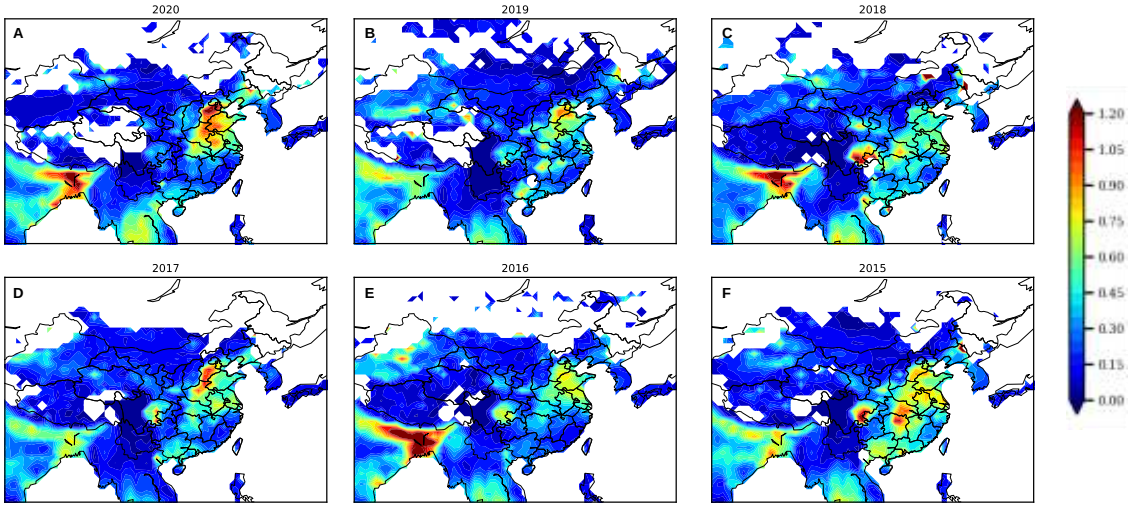

Fig. S4. MODIS L3 AOD from Terra and Aqua during the same three-week period with 2020-CLD from 2015 to 2020.

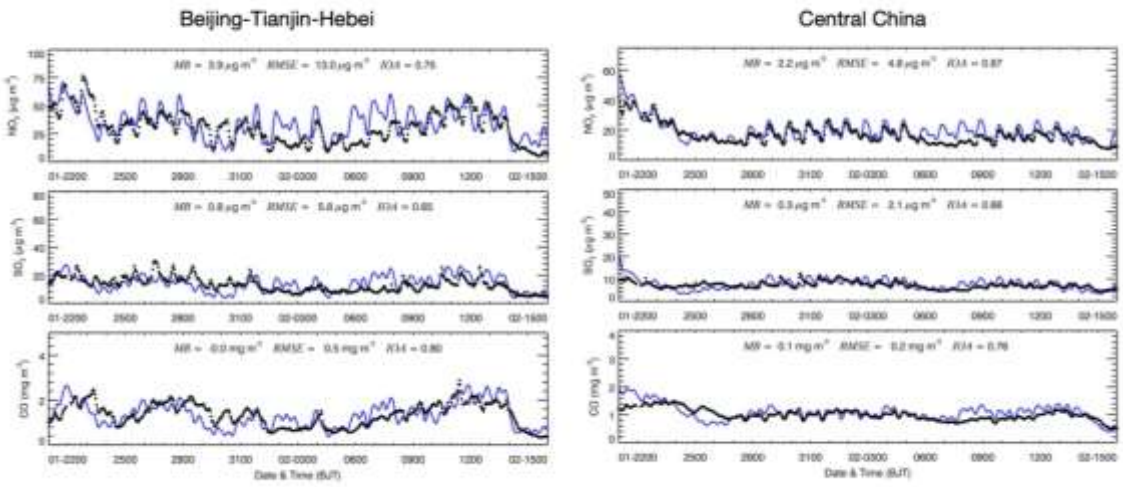

Fig. S5. Comparison of observed (black dots) and simulated (blue line) diurnal profiles of near surface hourly NO2, SO2, and CO averaged over all ambient monitoring stations in Beijing-Tianjin-Hebei (left panels) and Central China (Henan-Hubei-Hunan, right panels) from 21 January to 16 February 2020.

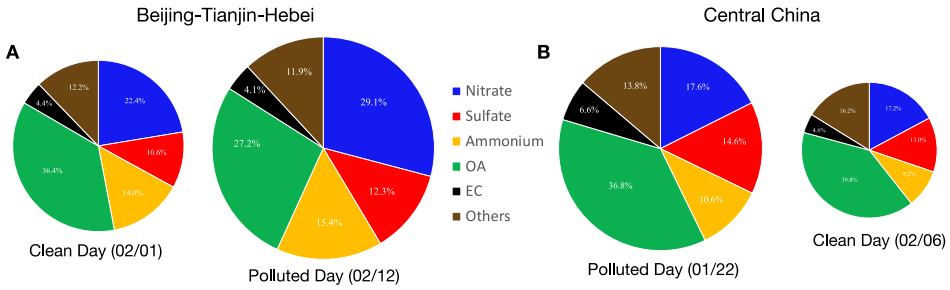

Fig. S6. WRF-Chem simulated surface aerosol species over two characteristic regions: Beijing-Tianjin-Hebei in northern China and Central China. OA and EC are short for organic aerosol and elementary carbon, respectively.

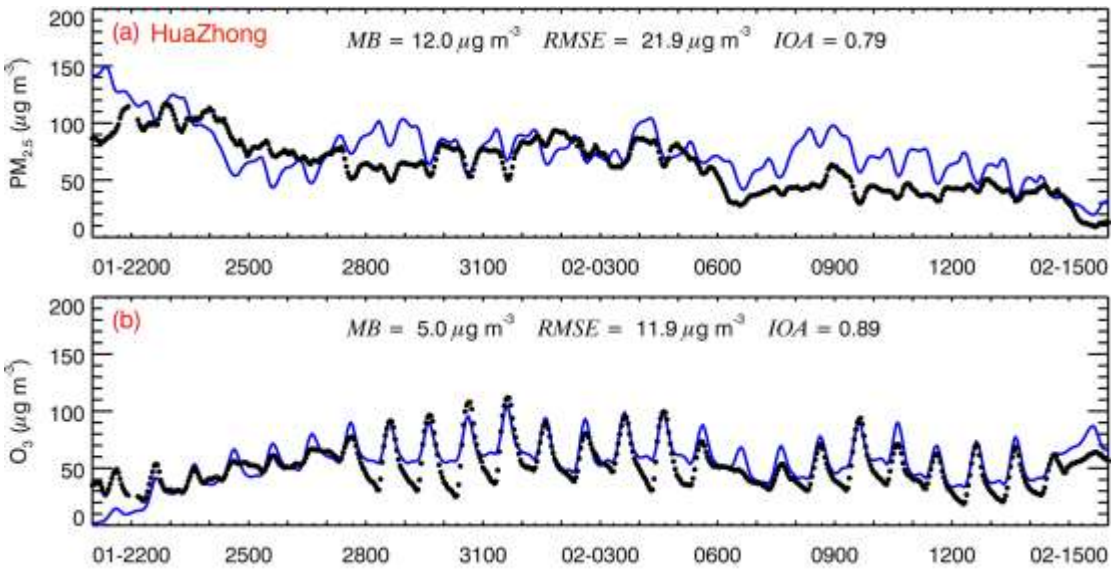

Fig. S7. WRF-Chem simulated time evolutions of PM2.5 and ozone in Central China. Black dots are observations, and blues lines are model simulations.

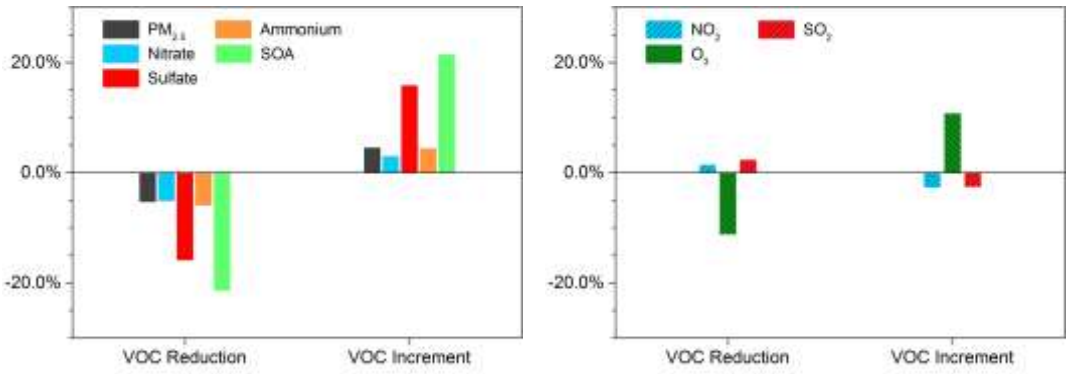

Fig. S8. Simulated sensitivity of aerosol species and precursor gases to the VOC changes by 30%.

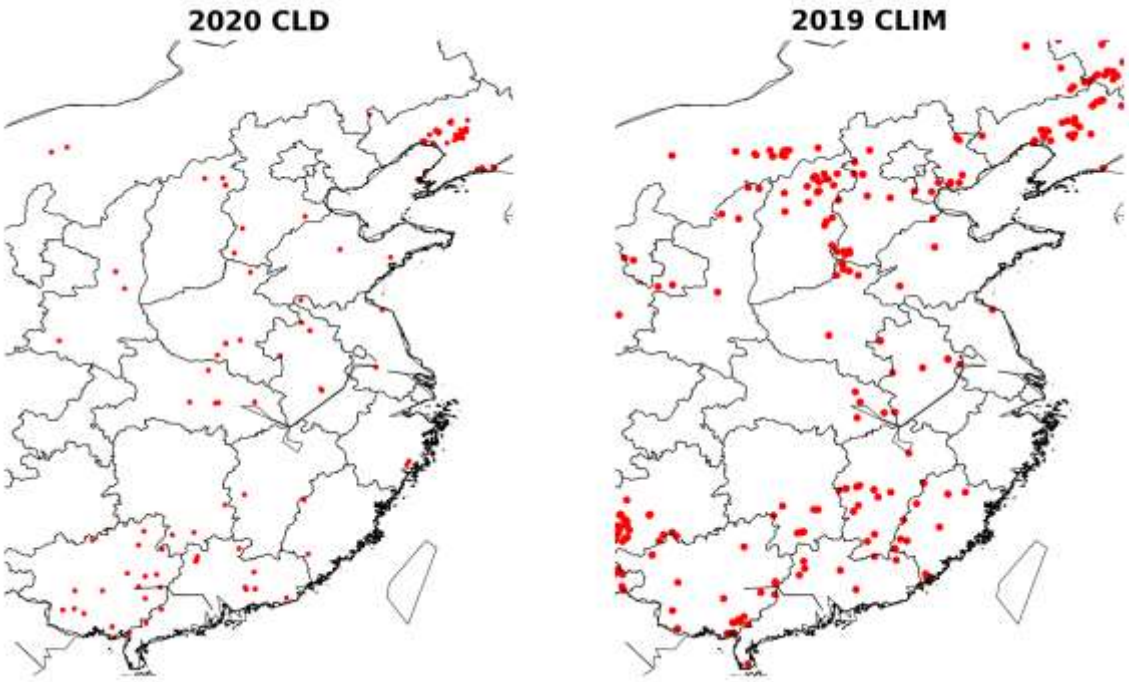

Fig. S9. Accumulated fire counts based on MODIS Active Fire Products over three-week periods during 2020-CLD and 2019-CLIM. Fire counts can be used to indicate the biomass burning in the agricultural activities. Dots in the plots are with confidence level larger than 80 in the MODIS product.

Table S1. National Air Quality Monitoring Stations

Station ID	Station Name	City	Longitude	Latitude	Station ID	Station Name	City	Longitude	Latitude
1001A	Wan Shou Xi Gong	Beijing	116.366	39.867	1325A	Dong Hu Li Yuan	Wuhan	114.367	30.572
1002A	Ding Ling	Beijing	116.17	40.287	1326A	Han Yang Yue Hu	Wuhan	114.251	30.551
1003A	Dong Si	Beijing	116.434	39.952	1327A	Han Kou Hua Qiao	Wuhan	114.284	30.62
1004A	Temple of Heaven	Beijing	116.434	39.875	1328A	Wu Chang Zi Yang	Wuhan	114.301	30.549
1005A	Agriculture Exhibition Center	Beijing	116.473	39.972	1329A	Qing Shan Gang Hua	Wuhan	114.427	30.61
1006A	Guan Yuan	Beijing	116.361	39.943	1330A	Tun Kou New District	Wuhan	114.153	30.475
1007A	Wan Liu Haidian District	Beijing	116.315	39.993	1331A	Han Kou Jiang Tan	Wuhan	114.301	30.595
1008A	Xincheng Shunyi	Beijing	116.72	40.144	1332A	Dong Hu Gao Xin	Wuhan	114.389	30.482
1009A	Huai Rou Town	Beijing	116.644	40.394	1333A	Wu Jia Shan	Wuhan	114.213	30.641
1010A	Chang Ping Town	Beijing	116.23	40.195	1334A	Chen Hu Qi Hao	Wuhan	113.853	30.3
1011A	Olympic Center	Beijing	116.407	40.003	1345A	Guang Ya Middle School	Guangzhou	113.235	23.142
1012A	Ancient city	Beijing	116.225	39.928	1346A	Guangzhou No.5 High School	Guangzhou	113.261	23.105
1141A	Pu Tuo	Shanghai	121.4	31.238	1348A	Guang Dong Business College	Guangzhou	113.348	23.092
1142A	Shi Wu Chang	Shanghai	121.478	31.204	1349A	Guangzhou No.86 High School	Guangzhou	113.433	23.105
1143A	Hong Kou	Shanghai	121.467	31.301	1350A	Fan Yu Middle School	Guangzhou	113.352	22.948
1144A	Shanghai Normal University in Xuhui	Shanghai	121.412	31.165	1351A	Hua Du Normal University	Guangzhou	113.215	23.392

1145 A	Yang Pu Si Piao	Shangha i	121.536	31.266	1352 A	Guangzho u Monitorin g Station	Guangzho u	113.26	23.133
1146 A	Qing Pu Dian Shan Lake	Shangha i	120.978	31.094	1353 A	Jiu Long Town Zhen Long	Guangzho u	113.568	23.278
1147 A	Jing An Monitorin g Station	Shangha i	121.425	31.226	1354 A	Lu Hu	Guangzho u	113.281	23.157
1148 A	Pu Dong Chuan Sha	Shangha i	121.703	31.191	1355 A	Mao Feng Shan Forestry Park	Guangzho u	113.589	23.554
1149 A	Pu Dong New District Monitorin g Station	Shangha i	121.533	31.228	2846 A	Ti Yu Xi	Guangzho u	113.321	23.132
1150 A	Pu Dong Zhang Jiang	Shangha i	121.577	31.207					

Table S2. WRF-Chem model configurations.

Region	East Asia
Simulation period	2020-01-21 to 2020-02-16
Domain size	400 × 400
Domain center	35.0°N, 114.0°E
Horizontal resolution	12km × 12km
Vertical resolution	35 vertical levels with a stretched vertical grid with spacing ranging from 30m near the surface, to 500m at 2.5km and 1km above 14km
Microphysics scheme	WSM 6-class graupel scheme *(36*)
Boundary layer scheme	MYJ TKE scheme *(37)*
Surface layer scheme	MYJ surface scheme *(37)*
Land-surface scheme	Unified Noah land-surface model *(38)*
Long-wave radiation scheme	Goddard longwave scheme *(39)*
Short-wave radiation scheme	Goddard shortwave scheme (*40)*
Meteorological boundary and initial conditions	NCEP 1°×1° reanalysis data
Chemical initial and boundary conditions	MOZART 6-hour output *(41)*
Anthropogenic emission inventory	SAPRC-99 chemical mechanism emissions (*30*)
Biogenic emission inventory	MEGAN model developed by (*31*)
Model spin-up time	24 hours

Table S3. Model sensitivity experiment description.

Experiments	***Configuration***	***Purpose***
Baseline	Described in Table S2.	To reproduce observed pollution changes.
Clim_Met	Using Climatological meteorological initial and boundary conditions averaged over the same time periods during 2015 - 2019.	To assess the meteorological influence on pollution changes.
NOx_80	According to the satellite observations, increasing NOx emissions in all sectors by 80% from the baseline simulation to reflect the non-COVID19 scenario.	To assess effect of NOx reduction.
Heteoro_Chem	Turning off all heterogeneous chemistry processes in our modified version of WRF-Chem.	To assess the contribution of heterogeneous chemistry to the haze formation.
VOC	Increasing/Decreasing VOC emissions by 30%.	To assess the sensitivity of VOC emissions to the haze formation.

References and Notes

1. Z. An, R.-J. Huang, R. Zhang, X. Tie, G. Li, J. Cao, W. Zhou, Z. Shi, Y. Han, Z. Gu, Y. Ji, Severe haze in northern China: A synergy of anthropogenic emissions and atmospheric processes. *Proc. Natl. Acad. Sci. U.S.A.* **116**, 8657–8666 (2019). doi:10.1073/pnas.1900125116 Medline

2. B. Zhao, H. Zheng, S. Wang, K. R. Smith, X. Lu, K. Aunan, Y. Gu, Y. Wang, D. Ding, J. Xing, X. Fu, X. Yang, K.-N. Liou, J. Hao, Change in household fuels dominates the decrease in $PM_{2.5}$ exposure and premature mortality in China in 2005-2015. *Proc. Natl. Acad. Sci. U.S.A.* **115**, 12401–12406 (2018). doi:10.1073/pnas.1812955115 Medline

3. Q. Zhang, Y. Zheng, D. Tong, M. Shao, S. Wang, Y. Zhang, X. Xu, J. Wang, H. He, W. Liu, Y. Ding, Y. Lei, J. Li, Z. Wang, X. Zhang, Y. Wang, J. Cheng, Y. Liu, Q. Shi, L. Yan, G. Geng, C. Hong, M. Li, F. Liu, B. Zheng, J. Cao, A. Ding, J. Gao, Q. Fu, J. Huo, B. Liu, Z. Liu, F. Yang, K. He, J. Hao, Drivers of improved $PM_{2.5}$ air quality in China from 2013 to 2017. *Proc. Natl. Acad. Sci. U.S.A.* **116**, 24463–24469 (2019). doi:10.1073/pnas.1907956116 Medline

4. G. Li, N. Bei, J. Cao, J. Wu, X. Long, T. Feng, W. Dai, S. Liu, Q. Zhang, X. Tie, Widespread and persistent ozone pollution in eastern China during the non-winter season of 2015: Observations and source attributions. *Atmos. Chem. Phys.* **17**, 2759–2774 (2017). doi:10.5194/acp-17-2759-2017

5. K. Li, D. J. Jacob, H. Liao, L. Shen, Q. Zhang, K. H. Bates, Anthropogenic drivers of 2013-2017 trends in summer surface ozone in China. *Proc. Natl. Acad. Sci. U.S.A.* **116**, 422–427 (2019). doi:10.1073/pnas.1812168116 Medline

6. G. Wang, R. Zhang, M. E. Gomez, L. Yang, M. Levy Zamora, M. Hu, Y. Lin, J. Peng, S. Guo, J. Meng, J. Li, C. Cheng, T. Hu, Y. Ren, Y. Wang, J. Gao, J. Cao, Z. An, W. Zhou, G. Li, J. Wang, P. Tian, W. Marrero-Ortiz, J. Secrest, Z. Du, J. Zheng, D. Shang, L. Zeng, M. Shao, W. Wang, Y. Huang, Y. Wang, Y. Zhu, Y. Li, J. Hu, B. Pan, L. Cai, Y. Cheng, Y. Ji, F. Zhang, D. Rosenfeld, P. S. Liss, R. A. Duce, C. E. Kolb, M. J. Molina, Persistent sulfate formation from London Fog to Chinese haze. *Proc. Natl. Acad. Sci. U.S.A.* **113**, 13630–13635 (2016). doi:10.1073/pnas.1616540113 Medline

7. F. Zhang, Y. Wang, J. Peng, L. Chen, Y. Sun, L. Duan, X. Ge, Y. Li, J. Zhao, C. Liu, X. Zhang, G. Zhang, Y. Pan, Y. Wang, A. L. Zhang, Y. Ji, G. Wang, M. Hu, M. J. Molina, R. Zhang, An unexpected catalyst dominates formation and radiative forcing of regional haze. *Proc. Natl. Acad. Sci. U.S.A.* **117**, 3960–3966 (2020). doi:10.1073/pnas.1919343117 Medline

8. L. Mao, R. Liu, W. Liao, X. Wang, M. Shao, S. C. Liu, Y. Zhang, An observation-based perspective of winter haze days in four major polluted regions of China. *Natl. Sci. Rev.* **6**, 515–523 (2019). doi:10.1093/nsr/nwy118

9. S. Wang, M. Zhao, J. Xing, Y. Wu, Y. Zhou, Y. Lei, K. He, L. Fu, J. Hao, Quantifying the air pollutants emission reduction during the 2008 Olympic games in Beijing. *Environ. Sci. Technol.* **44**, 2490–2496 (2010). doi:10.1021/es9028167 Medline

10. K. Huang, X. Zhang, Y. Lin, The “APEC Blue” phenomenon: Regional emission control effects observed from space. *Atmos. Res.* **164–165**, 65–75 (2015). doi:10.1016/j.atmosres.2015.04.018

11. R. Meng, F. Zhao, K. Sun, R. Zhang, C. Huang, J. Yang, Analysis of the 2014 “APEC Blue” in Beijing Using More than One Decade of Satellite Observations: Lessons Learned from Radical Emission Control Measures. *Remote Sens.* **7**, 15224–15243 (2015). doi:10.3390/rs71115224

12. D.-Y. Gong, W. Wang, Y. Qian, W. Bai, Y. Guo, R. Mao, Observed holiday aerosol reduction and temperature cooling over East Asia. *J. Geophys. Res. Atmos.* **119**, 6306–6324 (2014). doi:10.1002/2014JD021464

13. J. H. Seinfeld, S. N. Pandis, *Atmospheric Chemistry and Physics: From Air Pollution to Climate Change* (John Wiley & Sons, 2016).

14. M. Levy, R. Zhang, J. Zheng, A. L. Zhang, W. Xu, M. Gomez-Hernandez, Y. Wang, E. Olaguer, Measurements of nitrous acid (HONO) using ion drift-chemical ionization mass spectrometry during the 2009 SHARP field campaign. *Atmos. Environ.* **94**, 231–240 (2014). doi:10.1016/j.atmosenv.2014.05.024

15. J. Wu, N. Bei, B. Hu, S. Liu, Y. Wang, Z. Shen, X. Li, L. Liu, R. Wang, Z. Liu, J. Cao, X. Tie, L. T. Molina, G. Li, Aerosol-photolysis interaction reduces particulate matter during wintertime haze events. *Proc. Natl. Acad. Sci. U.S.A.* **117**, 9755–9761 (2020). doi:10.1073/pnas.1916775117 Medline

16. X. Tie, R.-J. Huang, J. Cao, Q. Zhang, Y. Cheng, H. Su, D. Chang, U. Pöschl, T. Hoffmann, U. Dusek, G. Li, D. R. Worsnop, C. D. O’Dowd, Severe Pollution in China Amplified by Atmospheric Moisture. *Sci. Rep.* **7**, 15760 (2017). doi:10.1038/s41598-017-15909-1 Medline

17. Z. Li, Y. Wang, J. Guo, C. Zhao, M. C. Cribb, X. Dong, J. Fan, D. Gong, J. Huang, M. Jiang, Y. Jiang, S.-S. Lee, H. Li, J. Li, J. Liu, Y. Qian, D. Rosenfeld, S. Shan, Y. Sun, H. Wang, J. Xin, X. Yan, X. Yang, X. Yang, F. Zhang, Y. Zheng, East Asian Study of Tropospheric Aerosols and their Impact on Regional Clouds, Precipitation, and Climate (EAST-AIR$_{CPC}$). *J. Geophys. Res. Atmos.* **124**, 13026–13054 (2019). doi:10.1029/2019JD030758

18. Y. Wang, A. Khalizov, M. Levy, R. Zhang, New Directions: Light absorbing aerosols and their atmospheric impacts. *Atmos. Environ.* **81**, 713–715 (2013). doi:10.1016/j.atmosenv.2013.09.034

19. Y. Wang, P.-L. Ma, J. H. Jiang, H. Su, P. J. Rasch, Toward reconciling the influence of atmospheric aerosols and greenhouse gases on light precipitation changes in Eastern China. *J. Geophys. Res. Atmos.* **121**, 5878–5887 (2016). doi:10.1002/2016JD024845

20. S. Guo, M. Hu, J. Peng, Z. Wu, M. L. Zamora, D. Shang, Z. Du, J. Zheng, X. Fang, R. Tang, Y. Wu, L. Zeng, S. Shuai, W. Zhang, Y. Wang, Y. Ji, Y. Li, A. L. Zhang, W. Wang, F. Zhang, J. Zhao, X. Gong, C. Wang, M. J. Molina, R. Zhang, Remarkable nucleation and growth of ultrafine particles from vehicular exhaust. *Proc. Natl. Acad. Sci. U.S.A.* **117**, 3427–3432 (2020). doi:10.1073/pnas.1916366117 Medline

21. Y. Liu, Z. Ning, Y. Chen, M. Guo, Y. Liu, N. K. Gali, L. Sun, Y. Duan, J. Cai, D. Westerdahl, X. Liu, K. Xu, K. F. Ho, H. Kan, Q. Fu, K. Lan, Aerodynamic analysis of

SARS-CoV-2 in two Wuhan hospitals. *Nature* 10.1038/s41586-020-2271-3 (2020). doi:10.1038/s41586-020-2271-3 Medline

22. R. Zhang, Y. Li, A. L. Zhang, Y. Wang, M. J. Molina, Identifying airborne transmission as the dominant route for the spread of COVID-19. *Proc. Natl. Acad. Sci. U.S.A.* 10.1073/pnas.2009637117 (2020). doi:10.1073/pnas.2009637117 Medline

23. G. A. Grell, S. E. Peckham, R. Schmitz, S. A. McKeen, G. Frost, W. C. Skamarock, B. Eder, Fully coupled "online" chemistry within the WRF model. *Atmos. Environ.* **39**, 6957–6975 (2005). doi:10.1016/j.atmosenv.2005.04.027

24. G. Li, W. Lei, M. Zavala, R. Volkamer, S. Dusanter, P. Stevens, L. Molina, Impacts of HONO sources on the photochemistry in Mexico City during the MCMA-2006/MILAGO Campaign. *Atmos. Chem. Phys.* **10**, 6551–6567 (2010). doi:10.5194/acp-10-6551-2010

25. G. Li, N. Bei, X. Tie, L. Molina, Aerosol effects on the photochemistry in Mexico City during MCMA-2006/MILAGRO campaign. *Atmos. Chem. Phys.* **11**, 5169–5182 (2011). doi:10.5194/acp-11-5169-2011

26. G. Li, M. Zavala, W. Lei, A. Tsimpidi, V. Karydis, S. N. Pandis, M. Canagaratna, L. Molina, Simulations of organic aerosol concentrations in Mexico City using the WRF-CHEM model during the MCMA-2006/MILAGRO campaign. *Atmos. Chem. Phys.* **11**, 3789–3809 (2011). doi:10.5194/acp-11-3789-2011

27. G. Li, W. Lei, N. Bei, L. Molina, Contribution of garbage burning to chloride and PM 2.5 in Mexico City. *Atmos. Chem. Phys.* **12**, 8751–8761 (2012). doi:10.5194/acp-12-8751-2012

28. K. Foley, S. Roselle, K. Appel, P. Bhave, J. Pleim, T. Otte, R. Mathur, G. Sarwar, J. Young, R. Gilliam, C. G. Nolte, J. T. Kelly, A. B. Gilliland, J. O. Bash, Incremental testing of the Community Multiscale Air Quality (CMAQ) modeling system version 4.7. *Geosci. Model Dev.* **3**, 205–226 (2010). doi:10.5194/gmd-3-205-2010

29. A. Nenes, S. N. Pandis, C. Pilinis, ISORROPIA: A new thermodynamic equilibrium model for multiphase multicomponent inorganic aerosols. *Aquat. Geochem.* **4**, 123–152 (1998). doi:10.1023/A:1009604003981

30. Q. Zhang, D. G. Streets, G. R. Carmichael, K. He, H. Huo, A. Kannari, Z. Klimont, I. Park, S. Reddy, J. Fu, D. Chen, L. Duan, Y. Lei, L. T. Wang, Z. L. Yao, Asian emissions in 2006 for the NASA INTEX-B mission. *Atmos. Chem. Phys.* **9**, 5131–5153 (2009). doi:10.5194/acp-9-5131-2009

31. A. Guenther, T. Karl, P. Harley, C. Wiedinmyer, P. Palmer, C. Geron, Estimates of global terrestrial isoprene emissions using MEGAN (Model of Emissions of Gases and Aerosols from Nature). *Atmos. Chem. Phys.* **6**, 3181–3210 (2006). doi:10.5194/acp-6-3181-2006

32. H. S. Halliday, J. P. DiGangi, Y. Choi, G. S. Diskin, S. E. Pusede, M. Rana, J. B. Nowak, C. Knote, X. Ren, H. He, R. R. Dickerson, Z. Li, Using Short-Term CO/CO2 Ratios to Assess Air Mass Differences Over the Korean Peninsula During KORUS-AQ. *J. Geophys. Res. D* **124**, 10951–10972 (2019). doi:10.1029/2018JD029697

33. R.-J. Huang, Y. Zhang, C. Bozzetti, K.-F. Ho, J.-J. Cao, Y. Han, K. R. Daellenbach, J. G. Slowik, S. M. Platt, F. Canonaco, P. Zotter, R. Wolf, S. M. Pieber, E. A. Bruns, M. Crippa, G. Ciarelli, A. Piazzalunga, M. Schwikowski, G. Abbaszade, J. Schnelle-Kreis,

R. Zimmermann, Z. An, S. Szidat, U. Baltensperger, I. El Haddad, A. S. H. Prévôt, High secondary aerosol contribution to particulate pollution during haze events in China. *Nature* **514**, 218–222 (2014). doi:10.1038/nature13774 Medline

34. D. G. Streets, T. Canty, G. R. Carmichael, B. de Foy, R. R. Dickerson, B. N. Duncan, D. P. Edwards, J. A. Haynes, D. K. Henze, M. R. Houyoux, D. J. Jacob, N. A. Krotkov, L. N. Lamsal, Y. Liu, Z. Lu, R. V. Martin, G. G. Pfister, R. W. Pinder, R. J. Salawitch, K. J. Wecht, Emissions estimation from satellite retrievals: A review of current capability. *Atmos. Environ.* **77**, 1011–1042 (2013). doi:10.1016/j.atmosenv.2013.05.051

35. Y. Wang, S. Dörner, S. Donner, S. Böhnke, I. De Smedt, R. R. Dickerson, Z. P. Dong, H. He, Z. Q. Li, D. H. Li, D. Li, D. Liu, X. Ren, N. Theys, Y. Wang, Y. Wang, Z. Wang, H. Xu, J. Xu, T. Wagner, Vertical profiles of NO2, SO2, HONO, HCHO, CHOCHO and aerosols derived from MAX-DOAS measurements at a rural site in the central western North China Plain and their relation to emission sources and effects of regional transport. *Atmos. Chem. Phys.* **19**, 5417–5449 (2019). doi:10.5194/acp-19-5417-2019

36. S.-Y. Hong, J.-O. J. Lim, The WRF single-moment 6-class microphysics scheme (WSM6). *Asia-Pac. J. Atmospheric Sci.* **42**, 129–151 (2006).

37. Z. I. Janić, "Nonsingular implementation of the Mellor-Yamada level 2.5 scheme in the NCEP Meso model" (2001).

38. F. Chen, J. Dudhia, Coupling an advanced land surface–hydrology model with the Penn State–NCAR MM5 modeling system. Part I: Model implementation and sensitivity. *Mon. Weather Rev.* **129**, 569–585 (2001). doi:10.1175/1520-0493(2001)129<0569:CAALSH>2.0.CO;2

39. M.-D. Chou, M. J. Suarez, X.-Z. Liang, M. M.-H. Yan, C. Cote, "A thermal infrared radiation parameterization for atmospheric studies" (2001).

40. M.-D. Chou, M. J. Suarez, "A Solar Radiation Parameterization for Atmospheric Studies," Volume 15 (1999).

41. L. W. Horowitz, S. Walters, D. L. Mauzerall, L. K. Emmons, P. J. Rasch, C. Granier, X. Tie, J. Lamarque, M. G. Schultz, G. S. Tyndall, J. J. Orlando, G. P. Brasseur, A global simulation of tropospheric ozone and related tracers: Description and evaluation of MOZART, version 2. *J. Geophys. Res. D* **108**, 4784 (2003). doi:10.1029/2002JD002853